The Study of Siderophile Elements in Group IIC Iron Meteorites

Hope Tornabene

April 26, 2018

Advisor: Dr. Richard Walker

GEOL 394

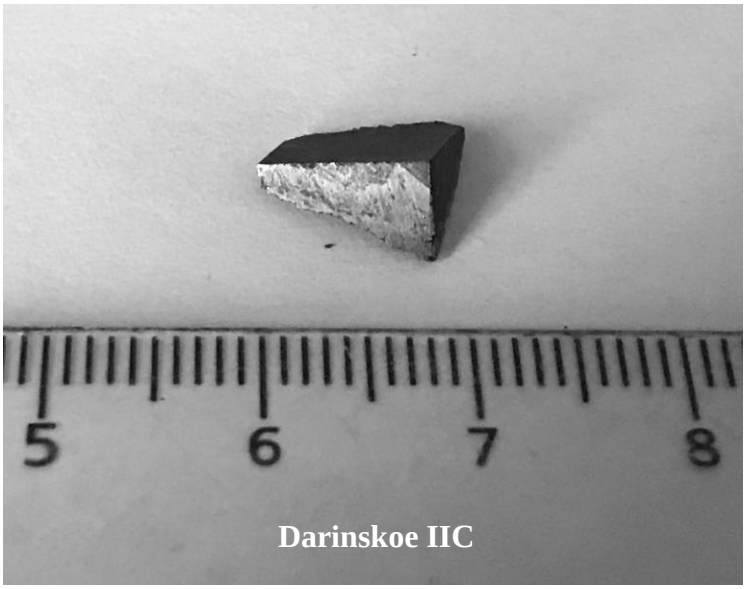

Darinskoe IIC

Abstract

The IIC iron meteorite group currently consists of eight meteorites. All eight were analyzed by laser ablation inductively-coupled plasma mass spectrometry (LA-ICP-MS) to determine bulk chemical composition. Most IIC iron meteorites exhibit similar chemical characteristics. There is a minor depletion in the more volatile siderophile elements relative to the more refractory siderophile elements. The IIC irons have similar, nested siderophile element abundance patterns, and variations in highly siderophile element abundances can be accounted for by a fractional crystallization model assuming initial S and P concentrations of 0.5 wt % and 5 wt %, respectively. Bulk highly siderophile element (HSE) concentrations reveal a distinct disparity between most IIC irons and Wiley, and also a sample of Cratheús received from the Field Museum. These results indicate that Wiley is not a IIC iron and likely formed on a separate parent body. The sample of Cratheús from the Field Museum is chemically different from other IIC irons, and is likely a misidentified sample of Cratheús (1931), which is a IVA iron meteorite.

1. Introduction

Meteorites are recovered fragments of small rocky objects in space called meteoroids. There are three general types of meteorites: iron, stony, and stony iron meteorites. Stony meteorites are composed of silicate materials. Stony irons consist of approximately equal proportions of metal and silicates. Iron meteorites contain 90-100% iron and nickel and primarily consist of two mineral phases, kamacite (Fe, Ni) and taenite (Fe, Ni). Kamacite is the iron rich phase with 5 to 10% nickel, and taenite is the high nickel phase with 30 to 70% nickel. Together, these phases can make up a Widmanstätten pattern, an essential characteristic in the classification of some iron meteorites.

Iron meteorite groups are comprised of what are believed to be genetically related iron meteorites. Meteorites within a group are likely formed in the same locality in the solar system and experienced a similar chemical and physical history on the same parent body (Scott and Wasson 1975). Iron meteorite groups are classified into two broad categories based on their believed mechanisms of formation: magmatic and non-magmatic meteorites. Magmatic meteorite groups have little variation in Ni and Ge concentrations. They are believed by many to have formed by fractional crystallization, fueled by the decay of the extinct isotope ^{26}Al. By contrast, non-magmatic iron meteorite groups exhibit large variations in Ni and Ge that cannot be explained by fractional crystallization. Non-magmatic meteorites likely formed by metal segregating from silicates within large melt sheets produced by the heat of impacts. Classification of iron meteorites is also dependent on volatile siderophile element (e.g., Ga, Ge) depletion within the meteorites. Roman numerals I-IV are used in the classification, I being the least depleted and IV being the most depleted in volatile siderophile elements. Additionally, classification of magmatic and non-magmatic iron meteorites is based on their mineralogic structure.

IIC iron meteorites are a magmatic group with little variation in Ga, Ge and Ni abundances. Previous studies indicate the IIC group formed as a result of fractional crystallization from a core with Ni, Ga, and Ge concentrated in the liquid and Ir in the solid (Wasson 1969). Eight meteorites have previously been classified as IIC iron meteorites. IIC irons have been rarely studied and only limited chemical data have been published for this group since the late 1960's.

Group IIC irons are structurally classified as plessitic octahedrites, indicating they have fine-grained mixture of kamacite and taenite. Furthermore, IIC irons are slightly depleted in Ga and Ge, hence their "II" classification.

In addition to classification based on chemical composition and texture, iron meteorites (and other meteorites) can be divided into two categories based on genetic isotopic characteristics.

Nucleosynthetic isotope anomalies of some elements, such as Mo, are used to place iron meteorites into carbonaceous chondrite (CC) and non-carbonaceous chondrite (NC) types. Nucleosynthesis is the process that creates new atomic nuclei. Different nucleosynthetic processes produce distinctive isotopic enrichments for some elements. Nucleosynthetic isotopic anomalies exhibit isotope ratios that differ from the average bulk silicate Earth. They presumably developed in meteorite parent bodies by heterogeneous distribution of presolar grains in the early nebular disk. Ruthenium and Mo isotope anomalies are especially prevalent in iron meteorites. Molybdenum isotopes are useful because they exhibit large and distinctive nucleosynthetic isotopic anomalies in bulk meteorites (Budde et al. 2016). The CC suite is distinguished from the NC suite due to an excess of r-process component (Poole et al. 2017). Additionally, Ru isotope ratios define a clear dichotomy useful for delineating the CC and NC groups. Carbonaceous chondrite and NC groups may have formed at two distinct times in the early solar system, which is reflected by ^{182}W isotope compositions (Krujier et al. 2017). More importantly, CC and NC groups likely formed in two separate locations in the solar nebula. Kruijer et al. (2017) suggested the CC type meteorites formed outboard of the proto-Jupiter. The IIC group is classified as CC type.

Iron meteorites provide insight into parental body and core composition, as well as the timing of core formation. Wasson (1969) reported data for Ni, Ga, Ge, and Ir for IIC irons. No subsequent chemical studies of the group have been published. Classification of these meteorites was primarily based on these elemental concentrations. It has recently been shown that the IIC group may be isotopically, and therefore genetically, distinct compared with other iron meteorite groups (Poole et al. 2017). For example, the IIC group exhibits the largest Mo isotope anomalies of any iron meteorite group analyzed to date (Poole et al. 2017). In addition, they also display an anomalous $^{183}W/^{184}W$ ratio relative to the rest of CC type irons (Kruijer et. al 2017). One meteorite from the IIC group, Wiley, is characterized by an even higher $^{183}W/^{184}W$ ratio than the other IIC meteorites (Kruijer et. al 2017), which suggests it may not be a member of the group.

2. Samples

Five samples have been obtained from the Smithsonian Institution National Museum of Natural History: Ballinoo (USNM 3284), 8.297g; Kumerina (USNM 5711), 6.813g; Perryville (USNM 428), 4.818g; Salt River (USNM 1131), 5.865g; and Wiley (USNM 1328), 9.390g. Cratheús (1950) (ME 2712), 0.320g was received from the Field Museum (Chicago). An additional sample of Cratheús (1950) and a IVA iron meteorite Pará de Minas were obtained from the Museu Nacional/UFRJ, Brazil. Unter Mässing (MPK 3074A), 4.720g was obtained from Senckenberg Forschungsinstitut und Naturmuseum, Germany and Darinskoe, >20g was received from Geological Museum of the Geological and Geophysical Institute of the Siberian Branch, Russia.

3. Objectives of Research

Current research indicates that each magmatic iron meteorite group is representative of a core derived from a distinct parent body. Therefore, analysis of IIC iron meteorite samples provide information regarding the relative siderophile element composition of the bulk parent body. Objectives are: first, measure the siderophile element abundances of each meteorite sample; second, measure the Re-Os isotopic systematics of each meteorite; third, model fractional crystallization; last, reversely model the bulk core composition.

The Re-Os isotope system has been used to constrain the ages of crystallization of several meteorite groups, e.g., IVB (Walker et al. 2008). To generate precise ages, however, substantial variation in Re/Os is required in order to define a precise isochron slope for the group. Even if

the variation in Re/Os is limited, the system can nevertheless be used to assess whether the HSE were open or closed to movement after crystallization. If an iron meteorite does not plot on a primordial isochron, then it is inferred that the meteorite has undergone secondary processes.

Specific hypotheses regarding the IIC group are as follows: 1) IIC iron meteorites can be related by crystal-liquid fractionation processes. 2) The modeled parent core has a chondritic relative abundance of the siderophile elements. 3) Wiley has chemical characteristics that are inconsistent with the IIC iron meteorites, indicating it formed on a different parent body.

4. Significance of Work

Analysis of the seldom studied group IIC irons aids in diminishing the ambiguity of Wiley's classification and provides new insights to the chemical composition and evolution of CC type parent bodies.

5. Methods

Laser ablation inductively-coupled plasma mass spectrometry *in situ* analysis of the siderophile elements Re, Os, W, Ir, Mo, Ru, V, Pt, Rh, Ni, Co, Fe, Pd, Cr, P, Mn, As, Au, Cu, Ge, Ge, and Zn, has been conducted on ten iron meteorites (Ballinoo, Cratheús (1950), Cratheús (Field Museum), Darinskoe, Kumerina, Pará de Minas, Perryville, Salt River, Wiley, and Unter Mässing). Additionally, high precision isotope dilution measurements of Re, Os, Ir, Ru, Pt and Pd have been performed on bulk samples (~50-100 mg) using ICP-MS and thermal ionization mass spectrometry (TIMS). Last, $^{187}Os/^{188}Os$ has been measured by TIMS.

Samples were carefully cut into small (~3-6 mm across) pieces with a diamond blade saw then polished with sand paper (400 abrasive particles per square inch) until one flat surface was free of diamond blade markings. Approximately 0.006-0.188 g (~2%) of the sample's mass may be lost during this process. The sample was ultrasonicated in ethanol, removing any contamination from the sawing and sanding. For each day of analysis siderophile element concentrations were measured along three lines by laser ablation. Each line was approximately 1mm long and 80μm wide for all samples (Fig. 1). For these lines, Laser ablation was achieved with a repetition rate of 7Hz, a total output of available energy of 58%, and an energy flux of ~2-4 Jcm^{-2}. The data from laser ablation was processed using *LAMTRACE* (Rusk 2009). The ratios of the intensity of the beam from the standard to the intensity of the beam from the sample were converted to calculate concentrations of Re, Os, W, Ir, Mo, Ru, V, Pt, Rh, Ni, Co, Fe, Pd, Cr, P, Mn, As, Au, Cu, Ge, Ge, and Zn, using Fe as an internal standard. The Fe concentration was determined for each meteorite by using accepted Ni and Co values in the literature (Wasson 1969) and assuming Ni, Fe, and Co compositions combined equal 100%. Measuring a wide range of elements requires the use of multiple, compositionally different external standards. The iron meteorites Filomena and Hoba were used as standards. The iron meteorite Babb's Mill [Troost] (ungrouped) was analyzed as an external standard to assess accuracy. The abundances of trace elements within the standards vary by orders of magnitude. For instance, Filomena has higher concentrations of Ga and Ge than Hoba. Due to the relatively high Ga and Ge concentrations in IIC irons, Filomena is a more appropriate

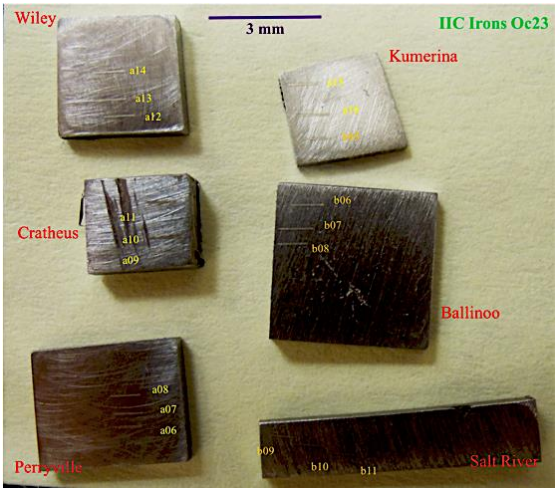

Figure 1. Six IIC iron meteorite samples after LA-ICP-MS

standard for measuring these elements than Hoba. Standard concentrations were matched to the IIC irons for the elements measured.

Next, small (~0.03373-0.12957 g) pieces of each sample were cut. A Re-Os mixed spike of 1324 ng/g Os and 330.5 ng/g Re was added to the samples. An appropriate amount of spike to add to each sample was calculated based on the concentration of Re obtained for each sample by ICP-MS. Then, a platinum group element (PGE) (Ir, Ru, Pt, Pd) mixed spike was added to each sample relative to the known concentration of Ir in the sample. Each mixture (sample and spike) was sealed, digested in Pyrex Carius tubes, and heated at approximately 230˚C for 24 hours. After each sample was heated, it was transferred to a centrifuge tube where carbon tetrachloride was added to each solution and shaken for one minute. Two separate phases formed: the aqueous phase that contained Re and all HSE except Os, and the dense carbon tetrachloride phase that contained the Os. The carbon tetrachloride was extracted with a pipette and added to concentrated hydrobromic acid. At that point, the Os favored the hydrobromic acid and the dense carbon tetrachloride was extracted and disposed of. The hydrobromic acid was dried down on a hot plate for several hours and purified Os was left in a small pinhead-sized dot. The Os was then analyzed by TIMS. Next, the phase with Re and the HSE was dried down on a hot plate for several hours. Then, it was diluted with low molarity hydrochloric acid and dried down again on the hot plate.

The remaining HSE were extracted and separated by anion exchange columns. Each sample was loaded into a column with 0.8 M HNO_3, then eluted with 12 mL 6 M HNO_3 for Re and Ru, 12 mL concentration HNO_3 for Ir and Pt, and 15 mL concentrated HCl for Pd. The elements were collected in separate teflon beakers, dried down, and additionally diluted ten-fold with 0.8 HNO_3. Rhenium, Ru, Ir, Pt and Pd were analyzed using inductively coupled plasma mass spectrometry.

6. Treatment of Uncertainties

Precision is determined by the standard deviation among multiple lines of data for a given meteorite (Table 1). Duplicate analyses of all the IIC irons have been conducted by laser ablation across the span of several days. Standard deviation (95% confidence) was calculated for multiple lines for a given meteorite by:

$$2(\sigma = \sqrt{\frac{[\sum(\bar{x}-x)^2]}{(n-1)}}) \quad (1)$$

where x-bar is the mean value of measurements, x is the individual measurement and n is the number of lines for each element per meteorite. For example, eight lines of measurements for Cratheús (1950), from Museu Nacional, Brazil, analyzed on different days indicate a range of 0.6 (Co) to 10.1 (Mo) percent deviation from the measured mean (Fig. 2). Each line measured for Cratheús (1950) and 2σ are shown in Table 1.

Accuracy is determined by the comparison of the external standard data for Babb's Mill [Troost] to accepted concentrations. The variation in concentrations ranged from 0.9 (Ge) to 21.0 (W) percent deviation from the accepted values for Babb's Mill (Fig. 3). Each analysis and 2σ are given in Table 2. Variations in elements could be a result of sample heterogeneity or from systematic errors from the mass spectrometer.

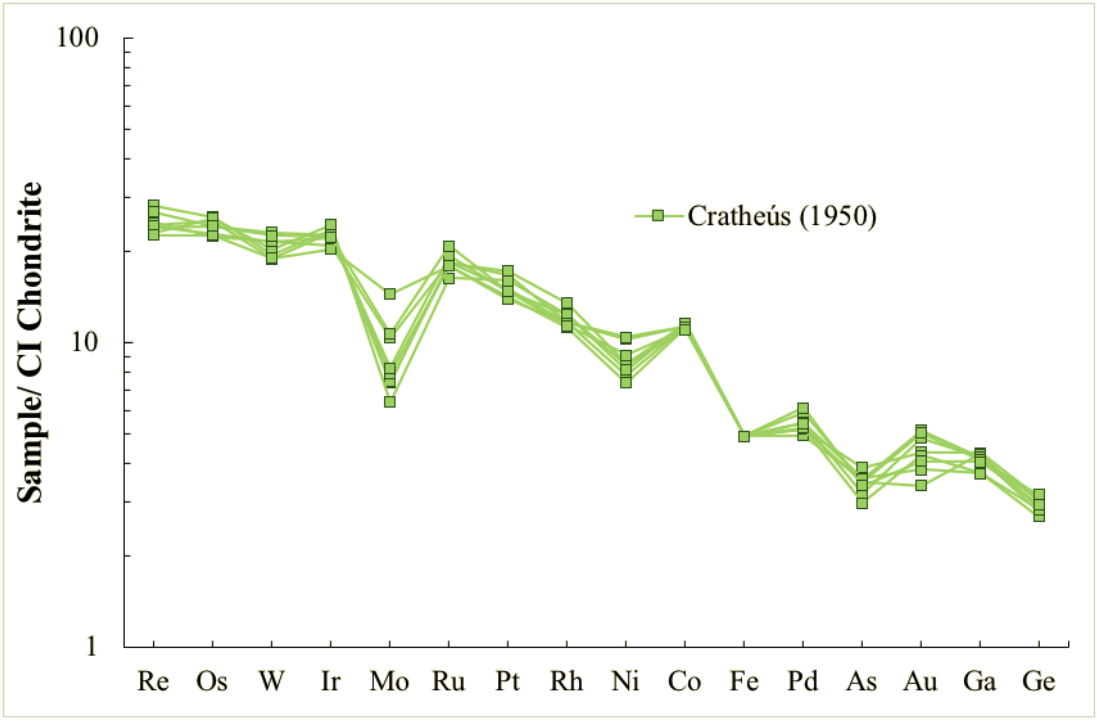

Figure 2. CI chondrite normalized abundance diagram of Cratheús (1950) to assess precision. Elements are in order of decreasing condensation temperature from left to right. Multiple lines indicate precision ranging from 0.6(Co) to 10.1(Mo) %.

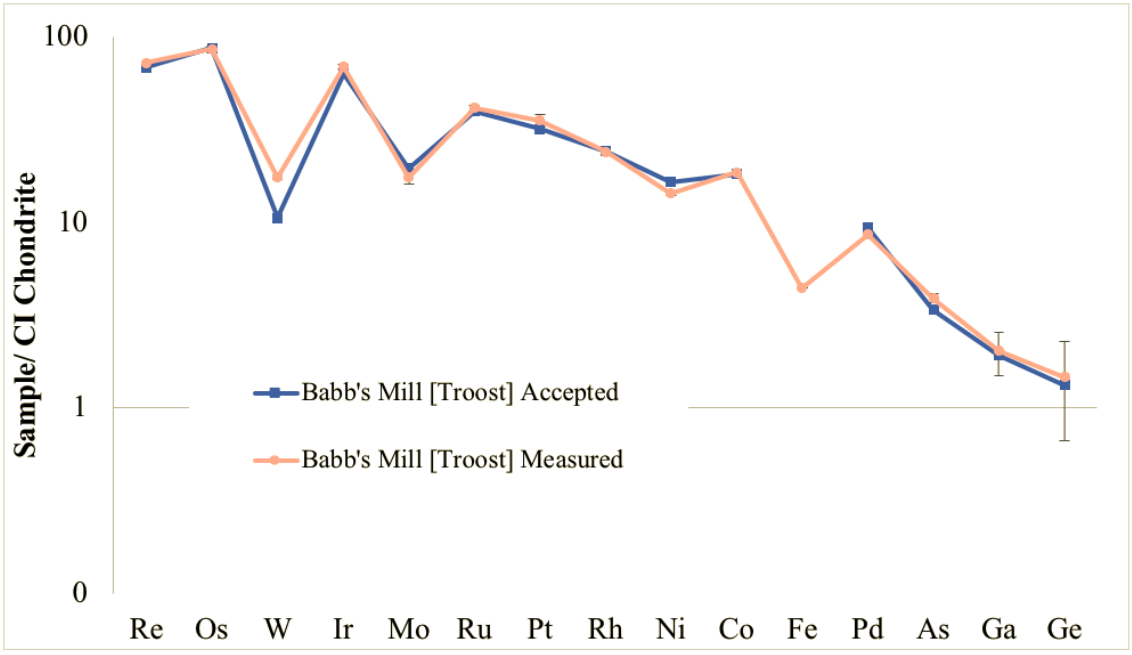

Figure 3. CI chondrite normalized abundance diagram of Babb's Mill [Troost] accepted and measured values to asses accuracy. Elements are in order of decreasing condensation temperature from left to right. Error bars are two standard deviation from the average measured values.

Table 1. Laser ablation inductively coupled plasma mass spectrometry data for Cratheús (19

Sample	Re	2σ	Os	2σ	W	2σ	Ir	2σ	Mo	2σ	Ru	2σ	Pt	2σ	Rh	2σ	Ni (%)	2σ	Co (%)	2σ	Fe (%)	2σ	Pd	2σ	As	2σ	Au	2σ	Ga	2σ	Ge	2σ
Cratheus (1950)	1.0		12.6		1.7		11.0		6.9		12.5		16.4		1.6		8.4		0.57		81.3		2.9		7.0		0.6		42.2		101.4	
	1.1		13.1		1.8		11.2		6.9		12.4		16.9		1.9		9.2		0.59		81.3		2.8		6.4		0.8		40.8		91.1	
	1.0		11.3		1.9		10.0		9.6		12.6		14.7		1.6		11.1		0.57		81.3		2.9		6.3		0.5		41.7		93.5	
	0.9		12.9		1.8		11.7		5.9		11.1		15.7		1.7		9.1		0.56		81.3		3.0		5.8		0.7		40.9		99.6	
	0.9		12.1		2.1		10.8		7.4		12.2		13.9		1.6		8.0		0.56		81.3		2.9		5.4		0.6		36.1		87.4	
	1.0		11.5		1.9		10.6		7.7		13.2		14.5		1.7		8.8		0.59		81.3		3.3		6.3		0.7		39.9		103.2	
	0.9		11.4		1.7		9.8		13		12.2		13.6		1.6		11.2		0.57		81.3		3.0		6.5		0.6		36.2		92.3	
	1.1		12.2		2.0		10.7		9.9		14.2		14.4		1.6		9.8		0.56		81.3		3.4		6.1		0.6		39.5		95.8	
Average	**1.0**	**± 0.1**	**12.2**	**± 0.5**	**1.9**	**± 0.1**	**10.7**	**± 0.5**	**8.5**	**± 1.7**	**12.5**	**± 0.6**	**15.0**	**± 0.8**	**1.7**	**± 0.1**	**9.4**	**± 0.8**	**0.57**	**± 0.01**	**81.3**	**± 0.0**	**3.0**	**± 0.2**	**6.2**	**± 0.3**	**0.6**	**± 0.1**	**39.7**	**± 1.7**	**95.5**	**± 3.9**

Ni, Co, and Fe concentrations reported in wt %, all others reported in µg/g

Table 2. Laser ablation inductively coupled plasma mass spectrometry data for Babb's Mill [Troost] standard.

Sample	Re	2σ	Os	2σ	W	2σ	Ir	2σ	Mo	2σ	Ru	2σ	Pt	2σ	Rh	2σ	Ni (%)	2σ	Co (%)	2σ	Fe (%)	2σ	Pd	2σ	As	2σ	Ga	2σ	Ge	2σ
Accepted Value																														
Babb's Mill [Troost]	2.7		44.1		1.0		30.6		18.2		27.2		31.4		3.4		17.8		0.9				5.2		6.1		18.7		43.3		
Measured	2.4		41.4		2.4		34.6		18.2		32.2		35.9		3.6		16.7		0.98		81.3		5.2		6.9		19.4		47.5	
	2.8		50.9		2.7		38.6		16.9		29.7		37.9		3.2		15.9		0.95		81.3		3.8		6.4		21.1		45.6	
	2.7		37.6		1.4		30.9		13.5		24.9		33.8		3.2		14.6		0.89		81.3		4.9		7.5		18.5		48.8	
	3.5		49.7		1.3		34.3		15.6		27.5		40.1		3.4		14.5		0.92		81.3		5.2		7.2		19.9		47.0	
	2.6		37.6		1.3		29.6		12.7		24.3		29.8		3.0		15.1		0.90		81.3		4.3		6.9		20.2		48.7	
	3.0		44.7		1.6		33.3		16.7		27.6		33.3		3.3		15.4		0.93		81.3		4.9		7.5		18.5		48.8	
	3.5		46.9		1.4		37.2		20.2		30.7		39.3		3.7		15.8		0.97		81.3		5.3		7.2		19.9		47.0	
	2.8		41.9		0.8		30.6		16.2		28.6		34.9		3.6		16.2		0.99		81.3		5.1		7.3		19.7		49.2	
	2.6		40.7		1.4		30.1		16.4		28.7		28.1		3.2		15.3		0.93		81.3		4.2		6.9		20.2		48.7	
Average	**2.9**	**± 0.3**	**43.5**	**± 3.3**	**1.6**	**± 0.4**	**33.2**	**± 2.1**	**16.3**	**± 1.5**	**28.2**	**± 1.7**	**34.8**	**± 2.7**	**3.4**	**± 0.2**	**15.5**	**± 0.5**	**0.94**	**± 0.02**	**81.3**	**± 0.0**	**4.8**	**± 0.4**	**7.1**	**± 0.2**	**19.7**	**± 0.5**	**47.9**	**± 0.8**

Ni, Co, and Fe concentrations reported in wt %, all others reported in µg/g

To demonstrate reproducibility, Darinskoe and a duplicate analysis are plotted on a CI chondrite normalized abundance plot (Fig. 4). The two measurements indicate maximum 2.7 (Ir and Pt) percent deviation for the HSE (Table 3).

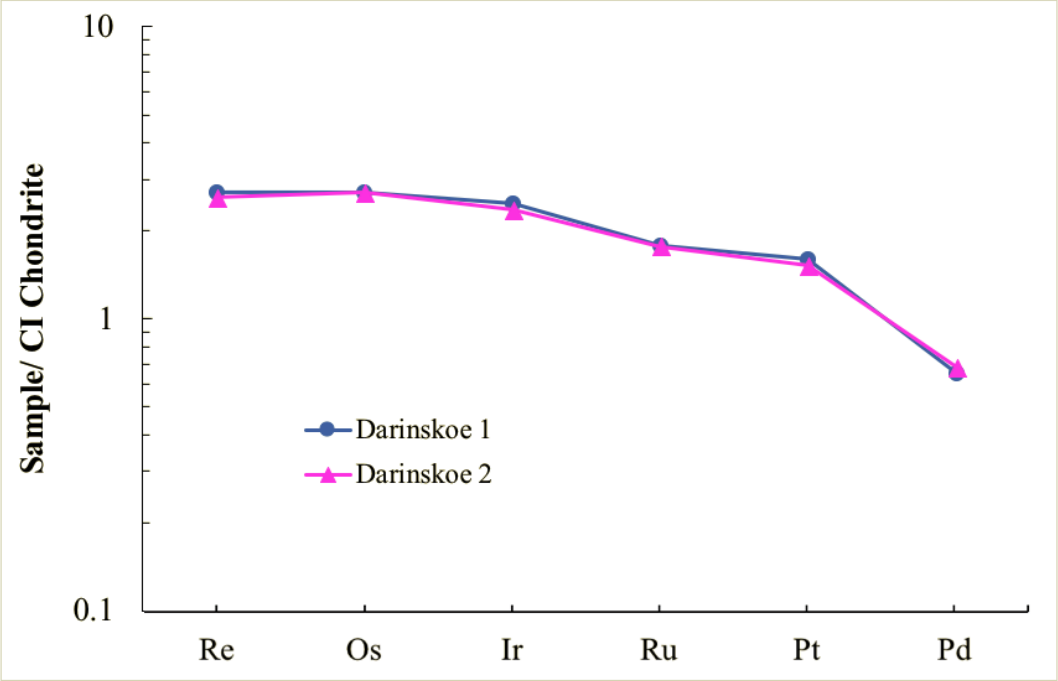

Figure 4. CI chondrite normalized abundance diagram of Darinskoe repeated measurements to demonstrate reproducibility. Elements are in order of decreasing condensation temperature from left to right. Data measured by isotope diltuion.

Table 3. HSE isotopic composition for Darinskoe obtained by isotope dilution.

Sample	**Re**	**Os**	**Ir**	**Ru**	**Pt**	**Pd**
Darinskoe 1	0.11	1.38	1.20	1.22	1.58	0.36
Darinskoe 2	0.10	1.37	1.13	1.21	1.50	0.38

Concentrations reported in ng/g.

7. Results

Average elemental concentrations obtained by LA-ICP-MS and 2σ variations for multiple lines of analysis are given in Table 4. As mentioned above, IIC irons are classified as plessitic octahedrites (kamacite spindle widths 60-70 microns). Therefore, laser ablation measurements across a sample are interpreted to be representative of bulk meteorite composition. The 2σ variations are < 15.3% deviation for all elements. Higher precision HSE concentrations for bulk samples obtained by isotope dilution are presented in Table 5.

Concentrations of Au for Kumerina and Cratheús (Field Museum) are omitted in Table 4 due to inaccurate measurements analyzed by laser ablation for that day. The measured Au concentrations for each line of Babb's Mill [Troost] did not match the accepted values. Additionally, the measured Au concentrations for Kumerina did not match Au concentrations for the IICs measured by Fouché and Smales (1966). It was concluded the Au concentrations for that day were inaccurate and therefore omitted.

While conducting laser ablation, spikes in the P concentrations were directly correlated with visible phosphide veins present in the samples. Siderophile elements are in very low abundances in phosphides, so the average concentrations across a line will be low. This can account for the slight heterogeneity across lines and the elevated 2σ values. Additionally, schreibersite ($[Fe,Ni]_3P$) is believed to be present in all IIC irons (Buchwald, 1975). The presence of schreibersite is likely the cause of the variation in W (Fig. 5) due to its tendency to partition with P. Additionally, Buchwald (1975) reported the IIC irons also having troilite (FeS) nodules. The presence of troilite and schreibersite are direct evidence that S and P were once present in the parent body. During fractional crystallization, concentrations of S and P influence the partitioning of elements (Chabot and Jones 2003). Consequently, S and P concentrations are estimated and utilized in modeling the parent body composition, discussed below.

The averaged data for most IIC irons show a slight depletion in volatile siderophile elements relative to refractory siderophile elements (Fig. 5). Bulk composition data from laser ablation normalized to CI chondrites, exhibit broadly similar patterns for most IIC irons as shown in Figure 5. Wiley, Cratheús (Field Museum) and Pará de Minas are characterized by significantly different patterns compared to the other samples.

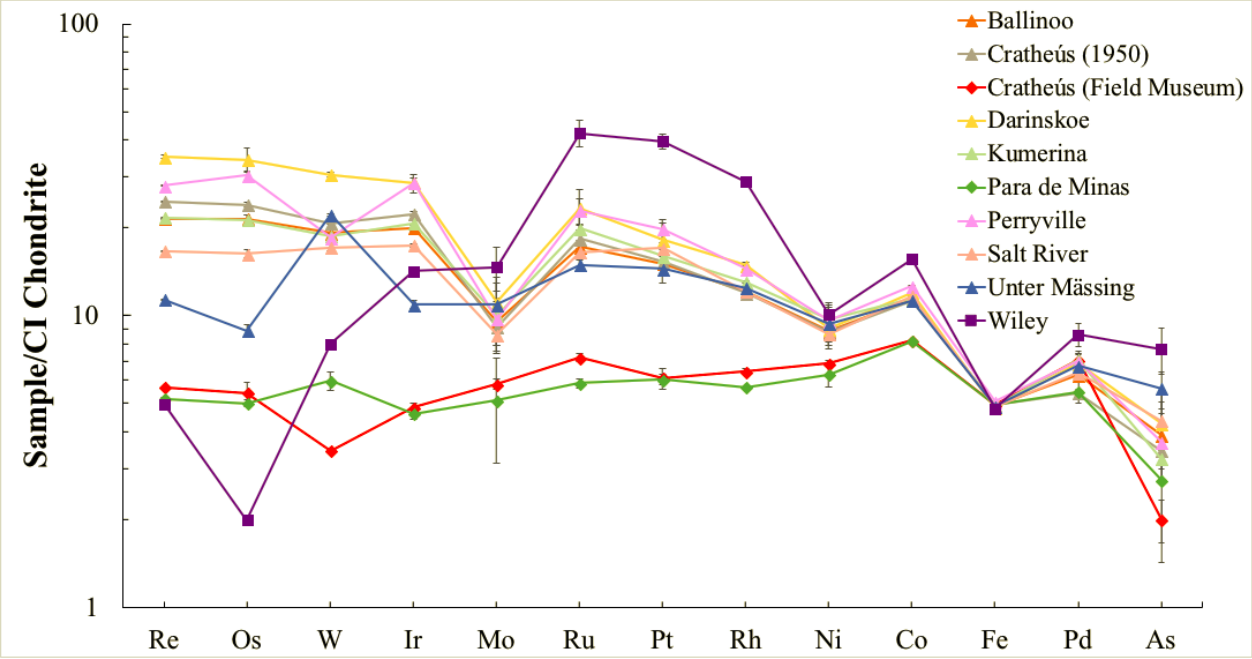

Figure 5. Bulk CI chondrite normalized abundance plot of the IIC irons, Wiley, Cratheús (Field Museum) and Pará de Minas (IVA irons). Elements are in order of decreasing condensation temperatures from left to right. Error bars are 2σ from the mean of multiple lines of measurements.

Table 4. Average elemental concentrations obtained by LA-ICP-MS

Sample	Re	2σ	Os	2σ	W	2σ	Ir	2σ	Mo	2σ	Ru	2σ	Pt	2σ	Rh	2σ	*n*
Darinskoe	1.4	± 0.5	17.4	± 3.2	2.8	± 0.6	13.7	± 2.1	10.3	± 1.8	15.9	± 3.7	17.8	± 2.6	2.1	± 0.4	*5*
Cratheús (1950)	1.0	± 0.1	12.2	± 0.5	1.9	± 0.1	10.7	± 0.4	8.5	± 1.7	12.5	± 0.6	15.0	± 0.8	1.7	± 0.1	*8*
Perryville	1.1	± 0.1	15.3	± 1.2	1.7	± 0.6	13.7	± 1.2	9.0	± 1.8	15.7	± 2.3	19.5	± 1.5	2.0	± 0.3	*6*
Ballinoo	0.8	± 0.1	10.9	± 0.7	1.7	± 0.5	9.6	± 0.4	8.9	± 1.7	11.8	± 0.9	14.8	± 0.5	1.7	± 0.1	*7*
Kumerina	0.9	± 0.1	10.8	± 0.9	1.7	± 0.6	9.9	± 0.7	9.3	± 1.0	13.6	± 0.5	15.7	± 0.9	1.8	± 0.1	*6*
Salt River	0.7	± 0.1	8.2	± 0.5	1.5	± 0.5	8.4	± 0.2	8.0	± 1.1	11.3	± 0.4	16.7	± 0.8	1.7	± 0.1	*6*
Unter Massing	0.45	± 0.04	4.5	± 0.4	2.0	± 0.2	5.2	± 0.4	10.1	± 2.7	10.2	± 0.6	14.2	± 1.5	1.7	± 0.1	*13*
Wiley	0.2	± 0.1	1.0	± 0.1	0.7	± 0.2	6.8	± 0.4	13.6	± 2.5	28.9	± 4.4	38.9	± 2.4	4.0	± 0.4	*6*
Para de Minas	0.2	± 0.1	2.5	± 0.1	0.8	± 0.4	2.2	± 0.2	9.0	± 8.5	4.0	± 0.2	5.9	± 0.2	0.80	± 0.04	*4*
Cratheús (Field Museum)	0.22	± 0.02	2.8	± 0.5	0.3	± 0.1	2.3	± 0.2	5.4	± 0.2	4.9	± 0.2	6.0	± 0.5	0.9	± 0.1	*6*

Sample	Ni (%)	2σ	Co (%)	2σ	Fe (%)	2σ	Pd	2σ	As	2σ	Au	2σ	Ga	2σ	Ge	2σ	*n*
Darinskoe	9.7	± 1.3	0.61	± 0.04	89.0	± 0.0	3.8	± 0.6	7.7	± 1.1	0.8	± 0.1	49.2	± 4.7	112.4	± 16.2	*5*
Cratheús (1950)	9.4	± 0.8	0.57	± 0.01	91.0	± 0.0	3.0	± 0.2	6.2	± 0.3	0.6	± 0.1	39.7	± 1.7	95.5	± 3.9	*8*
Perryville	10.4	± 1.2	0.64	± 0.05	90.3	± 0.0	3.9	± 0.6	6.7	± 0.9	1.0	± 0.1	44.3	± 4.7	112.6	± 17.3	*6*
Ballinoo	9.5	± 0.7	0.57	± 0.02	90.4	± 0.0	3.5	± 0.4	7.1	± 1.2	0.8	± 0.0	41.4	± 2.0	100.8	± 4.9	*7*
Kumerina	10.5	± 1.0	0.58	± 0.01	90.3	± 0.0	3.9	± 0.4	5.8	± 0.2			41.9	± 0.1	107.5	± 0.1	*6*
Salt River	9.3	± 0.2	0.59	± 0.01	90.0	± 0.0	3.5	± 0.3	7.9	± 1.2	1.4	± 0.1	41.0	± 1.7	108.6	± 5.3	*6*
Unter Massing	10.1	± 1.1	0.57	± 0.01	90.2	± 0.0	3.7	± 0.3	10.2	± 0.8	1.7	± 0.4	39.7	± 1.5	102.9	± 2.6	*13*
Wiley	10.8	± 1.0	0.79	± 0.03	88.5	± 0.0	4.8	± 0.8	13.9	± 1.4	1.1	± 0.1	44.6	± 0.9	128.6	± 4.3	*6*
Para de Minas	6.8	± 0.6	0.41	± 0.01	91.5	± 0.0	3.0	± 0.5	4.9	± 1.3	0.9	± 0.1	3.7	± 1.6	8.8	± 0.0	*4*
Cratheús (Field Museum)	7.4	± 0.2	0.416	± 0.004	91.0	± 0.0	3.9	± 0.3	3.6	± 0.3			2.2	± 0.2	5.1	± 0.0	*6*

Ni, Co, and Fe concentrations reported in wt %, all others reported in μg/g

n represents the number of lines analyzed for each sample

Table 5.

HSE and Os isotopic composition data for IIC irons obtained by isotope dilution.

Sample	Wt.	Re	Os	Ir	Ru	Pt	Pd	$^{187}Re/^{188}Os$	2σ	$^{187}Os/^{188}Os$	2σ
Darinskoe	0.037	1089	13787	11970	12090	15780	3632	0.3767	0.0006	0.12380	0.00010
Duplicate	0.037	1047	13671	11340	12050	14960	3816	0.3655	0.0006	0.12396	0.00010
Cratheús (1950)	0.054	1046	13064	11310	11650	13830	3158	0.3815	0.0006	0.12426	0.00010
Perryville	0.091	973	12860	11170	11730	17404	3424	0.3645	0.0006	0.12471	0.00010
Ballinoo	0.130	791	10506	9234	10320	16310	3507	0.3626	0.0006	0.12418	0.00010
Kumerina	0.034	775	9942	8947	10540	16180	3343	0.3754	0.0006	0.12491	0.00010
Salt River	0.076	588	7002	7143	9737	15300	3494	0.4048	0.0006	0.12748	0.00010
Unter Massing	0.072	414	4113	5170	9441	11540	4056	0.4806	0.0006	0.13388	0.00010
Cratheús (1931)	0.088	251	2605	2444	4026	6664	3434	0.4649	0.0006	0.13229	0.00010
Para de Minas	0.059	248	2540	2402	4052	6245	3751	0.4660	0.0006	0.13227	0.00010
Wiley	0.092	192	1063	6949	25874	35052	4534	0.8720	0.0006	0.16504	0.00010

Samples are listed in order of decreasing Re concentrations.

Weight is in grams and HSE are ng/g

The data for Cratheús (Field Museum) revealed concentrations of Ir, Ga, and Ge that did not match the literature values for the Cratheús (1950) (Buchwald, 1975; Wasson 1969). This sample was identified as Cratheús (1950) in the Field Museum collection, but has a composition that instead matches data for Cratheús (1931), a IVA iron meteorite (Buchwald, 1975). Thus, this Cratheús (Field Museum) is likely mislabeled as Cratheús (1950) in the Field Museum collection. The curator from the National Museum Rio de Janiero, Brazil was contacted in regards to the Cratheús (1950) and (1931) meteorites. She suggested that Cratheús (1931) was actually a mislabeled sample of Pará de Minas, a IVA meteorite. Both Pará de Minas and the sample in their collection labeled Cratheús (1950) were received from the National Museum Rio de Janiero. The Cratheús (1950) from the National Museum Rio de Janiero, Brazil has a composition similar to the other IIC meteorites **(**Fig. 6) and is presumed to be correctly labled. Cratheús from the Field Museum and Pará de Minas have nearly identical HSE abundances (Fig. 6).

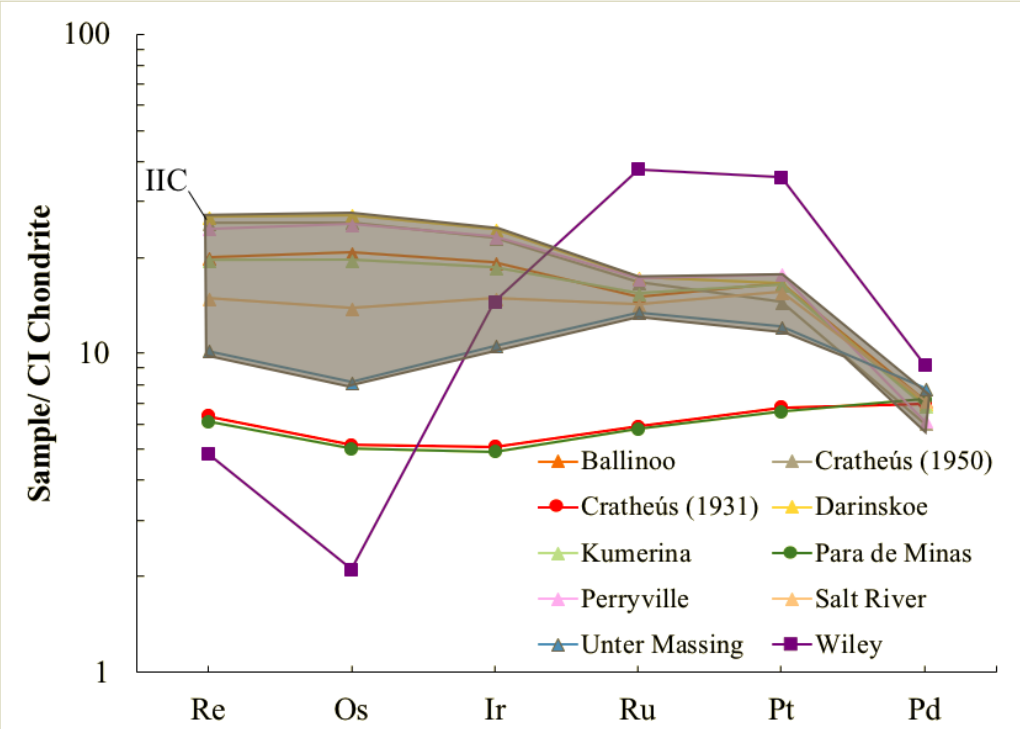

Figure 6. Bulk CI chondrite normalized abundance plot of HSE from isotope dilution. Figure in grey highlights the *bona fide* IIC irons.

The HSE abundance pattern for Wiley strongly deviates from the other IIC irons, especially in Ru and Pt abundances (Fig. 5 & 6). It also displays much higher concentrations of Ru, Pt, and Rh. As previously mentioned, Wiley has been found to have higher $^{183}W/^{184}W$ compared to the other IIC irons (Krujier et al. 2017). This is a nucleosynthetic ratio and indicative of a different parent body. Therefore, these data are consistent with hypothesis #3, that Wiley is not a IIC iron.

The high precision element abundance patterns for the *bona fide* IIC irons are characterized by decreasing abundances of Re, Os, Ir, Ru, and Pt, with little changes in Pd (Fig. 7). Of note, the HSE pattern for Ballinoo and Kumerina are almost identical. Additionally, Unter Mässing is depleted in Os by a factor 3 relative to Darinskoe.

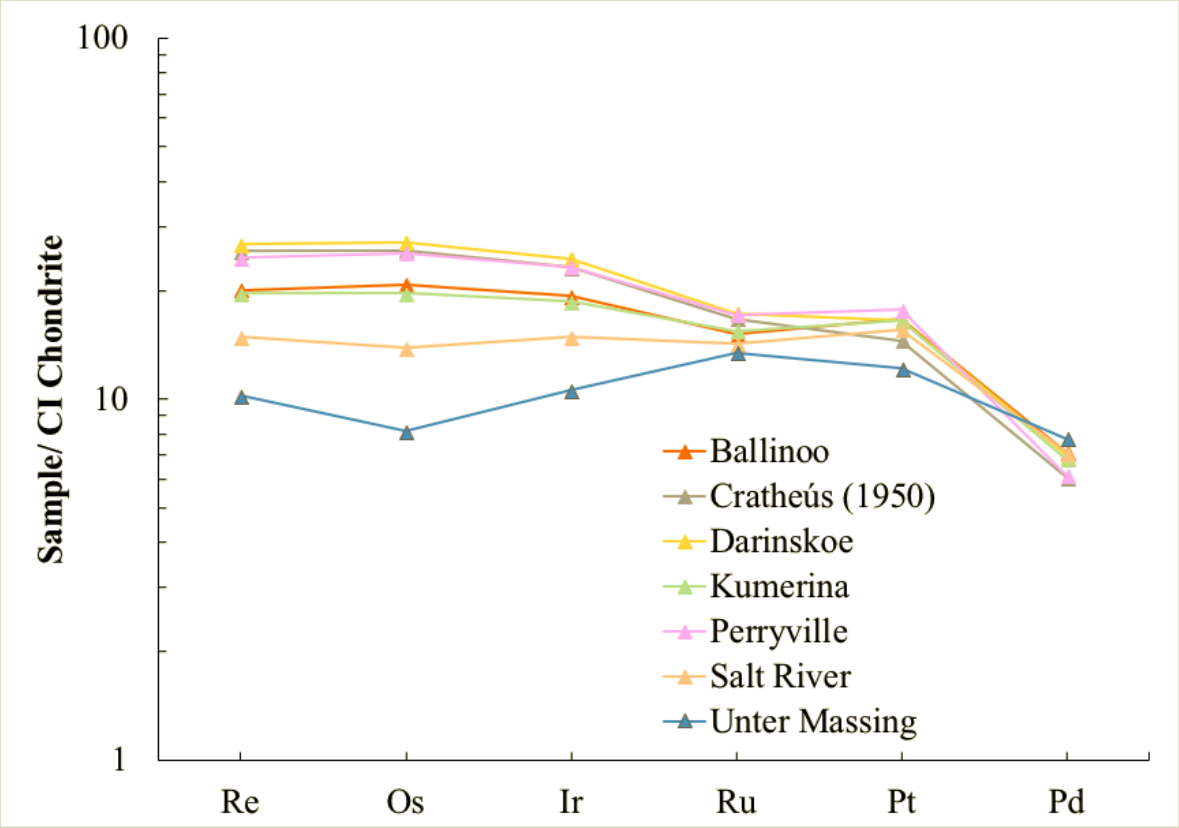

Figure 7. Bulk CI chondrite normalized abundance plot of HSE for the *bona fide* IIC irons. Darinskoe shows the highest Re concentration while Unter Mässing shows the lowest Re and Os concentrations indicating they are likely the least and most evolved IIC irons, repectively.

The IIC irons are characterized by a limited range in $^{187}Re/^{188}Os$ from 0.3626 to 0.4806 and $^{187}Os/^{188}Os$ from 0.1238 to 0.1339. Precision of the resulting isochron slope is limited. Most IIC irons fall along the primordial isochron indicating closed system behavior (Fig. 8). An initial $^{187}Os/^{188}Os = 0.0920 \pm 0.0057$, MSWD = 2.5, and an age of the IIC irons being 5044 ± 810 Ma was calculated using *ISOPLOT* (Ludwig 2003).

Highly correlated linear trends are seen on a log-log plot of Ir versus Re, Os, Ru, Pt, and Pd (Table 5; Fig. 9). Linear trends indicate the D values of the HSE changed in a constant relation with changes in D for Ir. Linear regressions and associated uncertainties of the log plots for the IIC irons were calculated using *ISOPLOT* (Ludwig 2003).

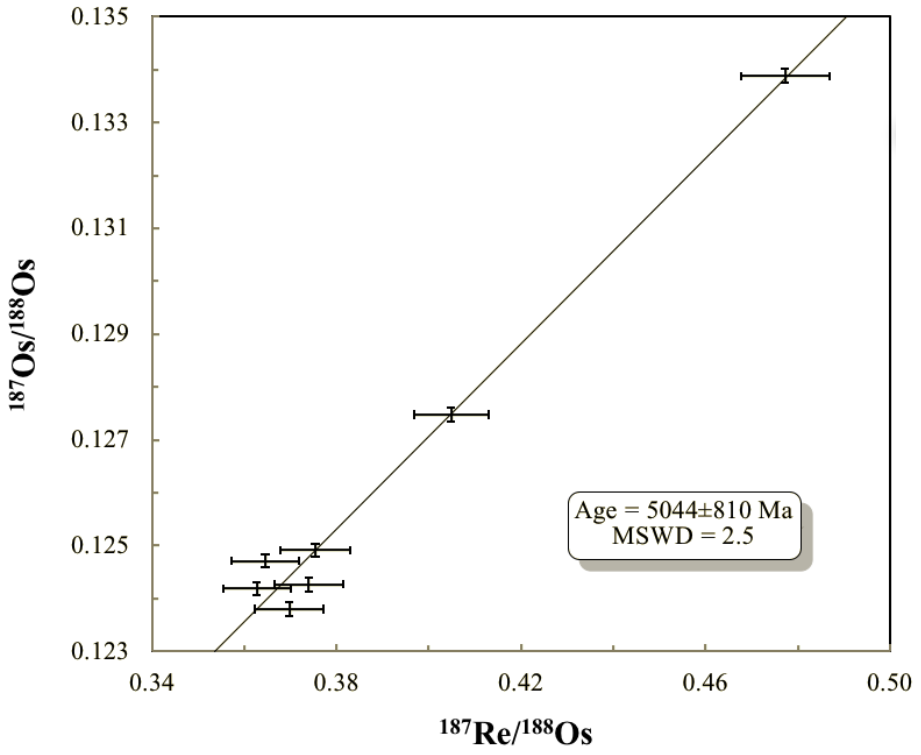

Figure 8. $^{187}Re/^{188}Os$ versus $^{187}Os/^{188}Os$ for IIC iron meteorites. MSDW is the mean squared deviates which is a measure of scatter about the regression. Error bars are two standard deviation.

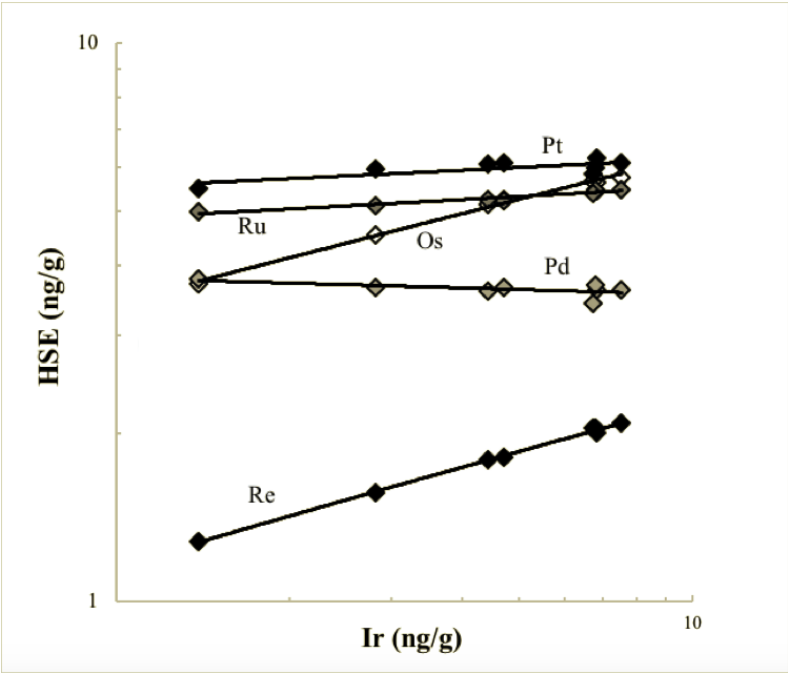

Figure 9. Logarithmic plot of Ir versus other HSE concentrations.

8. Parameterization

The process of reverse modeling entails using the least evolved iron meteorite within the IIC group to estimate the initial parent body composition. The iron with the highest Re and Os concentrations is defined as the least evolved. Darinskoe is the least evolved IIC iron meteorite. In order to estimate D (concentration ratio between solid metal and liquid metal) values for the HSE (Re, Os, Ru, Pt, and Pd), the D value for Ir is calculated by:

$$D = \frac{\frac{(1-2X_S-3X_P)}{(1-X_S-2X_P)}^{\beta-1}}{D_o} \quad (2)$$

where D_o is D in the end member non-metal-free Fe-Ni system, X_S is the mole fraction of S in the metallic liquid, X_P is the mole fraction of P in the metallic liquid, and β is a constant specific to the element being parametrized. The D value for Ir has been calculated using the parameterization method explained by Chabot and Jones (2003). Iridium is used to calculate the D values for HSE because its solid metal-liquid metal partitioning is the best experimentally constrained of all the HSE (Walker et al. 2008). The D values for the other HSE (Re, Os, Ru, Pt, and Pd) are estimated using the slope method (Chabot and Jones 2003):

$$Slope = \frac{[D(HSE)-1]}{[D(Ir)-1]} \quad (3)$$

where D(Ir) is the D value for Ir (calculated from equation 2) and *slope* is the slope of the line of best fit for a given element from Table 6. A constant D value for S of 0.001 is used and the D value for P is calculated using Eq. 2.

Table 6.
Linear regressions and uncertainties of log-log plots of HSE concentration data vs. Ir.

Element	Slope	2σ	MSWD
Re	1.16	0.12	0.13
Os	1.47	0.16	0.28
Ru	0.32	0.11	0.46
Pt	0.45	0.35	3.6
Pd	-0.17	0.12	1.9

Elements analyzed by isotope dilution. MSWD and 2σ calculated using *ISOPLOT*.

In order to estimate initial core concentrations for HSE, estimates for initial S and P concentrations are made. Changing D(Ir) values are calculated from the S and P concentrations at each increment of fractional crystallization and in turn, calculates the changing D(HSE) values over 0.1% increments of crystallization. The slope method is satisfactory due to the logarithmic plots of Ir versus Re, Os, Ru, Ir, Pt, and Pd defining highly-correlated linear trends in Figure 9 (Walker et al. 2008). The assumption that is being made when using the slope method is that the relative D values change throughout crystallization co-linearly (Walker et al. 2008).

Sulfur and P are highly incompatible elements with solid metal. As a result, they are concentrated in the melt and leave minimal (~300 ppm) trace in iron meteorite metal. Therefore, initial S and P concentrations need to be estimated. The P concentrations in IIC irons range from between 0.3 to 0.5 wt % (Goldstein and Doan 1972; Buchwald 1975). The assumption is made that the initial liquid S and P concentration was at least ten times that of the composition of the meteorite. The initial P concentration (5 wt %) was calculated by dividing the P composition of the meteorite (~0.3) by the constant D_o value for P (0.06). The variables for this model include the initial S and P concentrations and the starting HSE composition, representing the initial melt that the IIC irons crystallized from. Sulfur initial concentrations in the range of 0.01 to 3 wt % and P initial concentrations from 4 to 8 wt % were estimated for the model. The best fit initial set of parameters were 0.5 wt % S and 5 wt % P. With these parameters, initial Re concentrations are estimated assuming that the first crystallizing solids have a Re concentration similar to that of the least evolved meteorite, Darinskoe. Os concentrations are constrained assuming the Re/Os in the initial melt was similar to chondrites (~0.4). Rhenium and Os are used first because they are the best measured HSE. The rest of the HSE are constrained by varying initial concentrations to match those of the least evolved IIC, Darinskoe. The various models indicate that when less S (< 1 wt %) is initially present in the system, an intermediate degree (~40%) of fractional crystallization is needed in order to cover the diversity of HSE concentrations in the IIC irons (Fig. 10a-b).

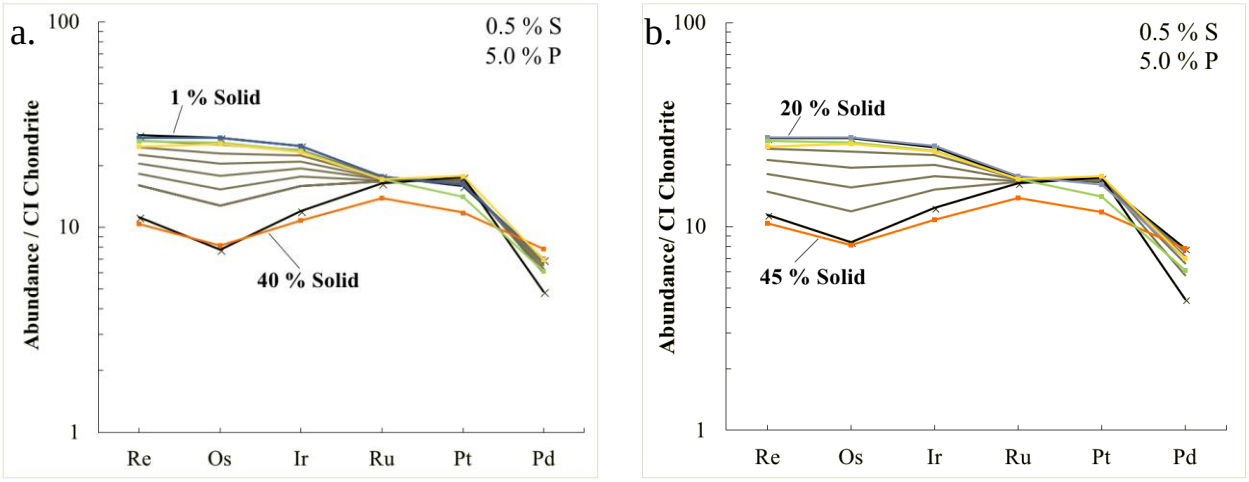

Figure 10a-b. CI chondrite normalized solid composition generated by fractional crystallization at 5 wt. % increments. Initial melt composition (Darinskoe) is in blue, Perryville in yellow, Cratheús (1950) in green, and the last solid to form (Unter Mässing) in orange.

Figure 10a-b presents the two evolution paths of fractional crystallization of the HSE concentrations. The first parameter (P1) considered is that Darinskoe represents the first solid crystallized from the initial melt. Darinskoe and Unter Mässing match 1% and 40% solid crystallization, respectively (Fig. 10a). Perryville and Cratheús (1950) match 5% solid crystallization (Fig. 10a). The estimated composition for the initial core melt has a chondritic pattern that is not unlike some enstatite chondrites (Fig. 11). Additionally, the estimated HSE composition of the parent core is approximately ten times that of chondrites indicating the core was approximately 10% the mass of the IIC parent body.

The second parameter (P2) considered is that the IIC irons represent an intermediate degree of fractional crystallization. Darinskoe was assumed to be representative of a solid crystallized

after 20% fractional crystallization. Darinskoe and Unter Mässing match 20 and 45% solid crystallization, respectively (Fig. 10b). Perryville and Cratheús (1950) match 25% solid crystallization (Fig. 10b). For P2, the calculated composition for the initial core melt has an almost perfect chondritic pattern (Fig. 11). In this case, the HSE composition indicates the core was 11% the mass of the IIC parent body. The initial concentrations of HSE calculated from these models for the IIC parent body core are given in Table 7 for both parameters.

Table 7.
Calculated intial concentrations (ng/g) for parameters discussed in the text

	Re	Os	Ir	Ru	Pt	Pd
P1	360	3970	4400	7750	11200	5400
P2	490	6050	5570	7850	11100	6450

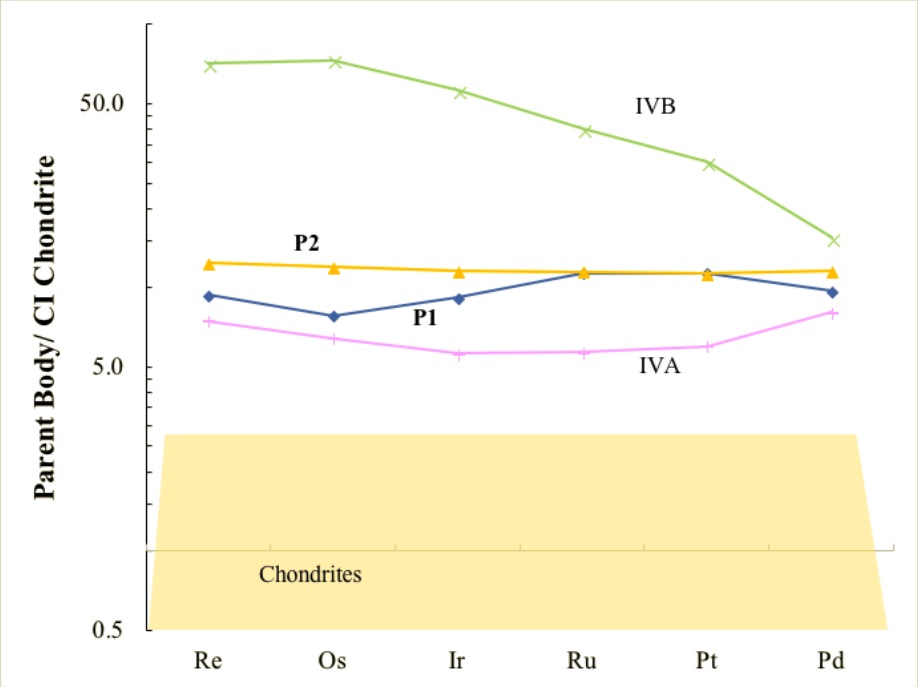

Figure 11. Plot of calculated parental melt concentrations of HSE, normalized to CI chondtites. The two parameter concentrations are plotted from Table 7. For comparison, the intial concentrations estimated by Walker et al. 2008 (IVB) and McCoy et al. (IVA) are shown.

Meteorites that have formed by fractional crystallization of a metallic core can represent solids directly precipitated from a liquid that they were in equilibrium with, equilibrium melt trapped in and mixed with solids, or a liquid composition preserved by entrapments in earlier formed solids (Wasson 1999; Walker et al. 2008). Fractional crystallization models of Re (ppb) versus $^{187}Re/^{188}Os$ are best utilized for this model because Os was the best measured of the HSE and Re/Os was used to estimate initial parent melt concentrations of HSE. The models of Re (ppb) versus $^{187}Re/^{188}Os$ can account for most IIC irons (Fig. 12a-d). The liquid track shown is the path of evolving liquid via fractional crystallization that is accompanied by the solid track. A meteorite that falls along the solid track will be representative of an equilibrium solid and one that falls between the tracks will represent a mixture of equilibrium solids and liquids. Mixing

curves (dashed lines) represent fractional crystallization at 10% (Fig. 12a) and 5% (Fig. 12b-d) increments.

For P1 (Fig. 12a), Darinskoe likely represents the first equilibrium solid to crystallize from the evolving liquid. Cratheús (1950) represents an early solid precipitated from the evolving liquid melt. The remaining irons that do not fall on mixing curves, but between the solid and liquid tracks, could represent mixtures of equilibrium solids and liquids at variable degrees of solid crystallization. Ballinoo, Kumerina, and Perryville plot below the mixing curve between initial melts and solids. Since P1 fractional crystallization model cannot account for Ballinoo, Kumerina, or Perryville the model is inconsistent with the IIC pattern.

For P2, all IIC irons can be accounted for by the fractional crystallization model (Fig. 12b). Darinskoe and Cratheús (1950) likely represent the first solids to form after 20% solid crystallization. Salt River and Unter Mässing fall along mixing curves and could represent mixtures of variable proportions of solid and liquid at 20% and 40% solid crystallization, respectively. Since Kumerina and Perryville do not fall on mixing curves, but fall between the solid and liquid tracks, they could represent mixtures of equilibrium solids and liquids at variable degrees of solid crystallization. No irons plot along the liquid track which would represent an equilibrium liquid composition.

An alternative parameter considered was a higher concentration of initial S. Figure 12c plots the IIC irons between solid and liquid tracks with 5 wt % initial S and 4 wt % initial P. In this case, Ballinoo, Kumerina, and Perryville all fall below the mixing curve between initial melts and solids. Therefore, fractional crystallization models with moderate S concentrations are inconsistent for the IIC irons.

For comparison, 0.5 wt % initial S and 8 wt % initial P were used as starting parameters for an additional model (Fig. 12d). Similarly, Ballinoo and Perryville fall below the mixing curve, indicating a higher P concentration is insufficient for modeling fractional crystallization of the IIC irons.

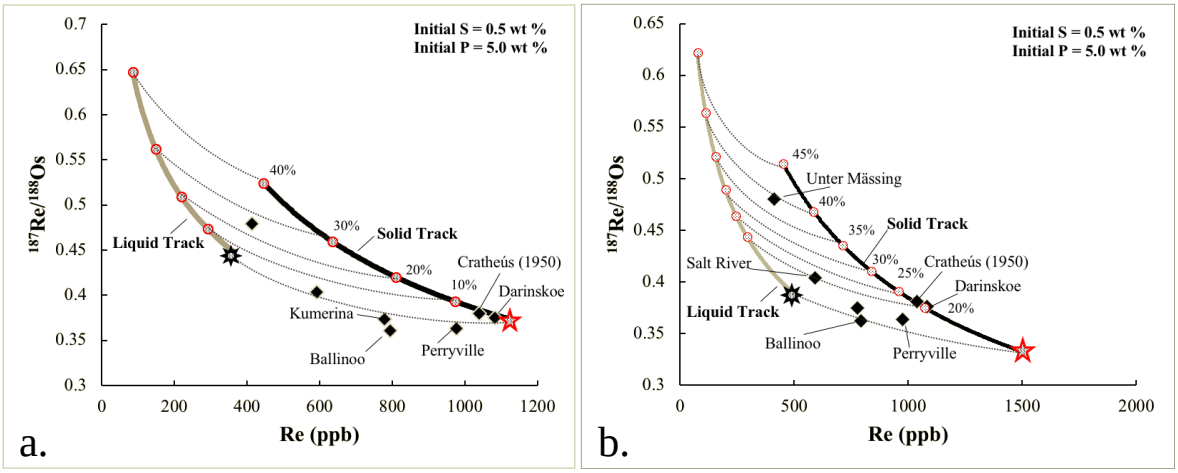

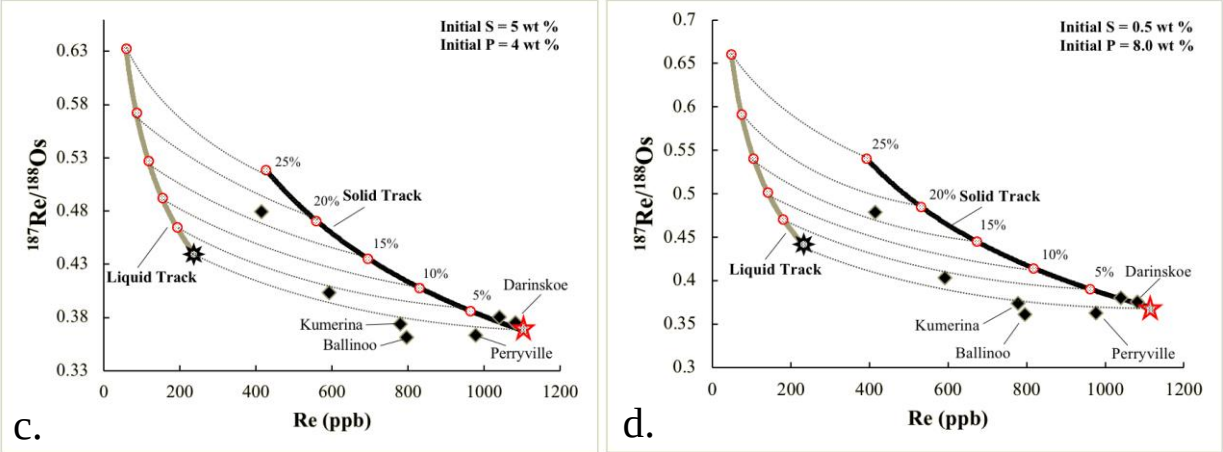

Figure 12a-d. Fractional crystallization model for Re (ppb) versus $^{187}Re/^{188}Os$ calculated for initial set of parameters defined by the assumed S and P concentrations discussed in the text. D(Re) and D(Os) were calculated by the slope method. The black diamonds are the data for the IIC irons. The black line represents the solid track and the grey line respresents the liquid track. The red circles show solid and liquid crystallization in 10% increments. The dotted lines are the mixing curves conncecting the equilibrium solid and liquid tracks at each increment. The red star represents the composition of the first solid to form. The black star represents the starting liquid composition.

9. Summary

Siderophile element abundances of ten meteorite samples were measured by LA-ICP-MS. Of the ten samples, Ballinoo, Cratheús (1950), Darinskoe, Kumerina, Perryville, Salt River, and Unter Mässing are consistent with being IIC iron meteorites. The data supports the hypothesis that Wiley has chemical characteristics inconsistent with being a IIC iron. The magmatic group can be successfully modeled from 20 to 45% solid fractional crystallization with 0.5 wt % initial S and 5 wt % initial P concentrations. Therefore, the IIC irons were derived from the same parent body. The modeled parent body core has a chondritic relative abundance of siderophile elements and was approximately 11% the mass of the parent body.

Works Cited

Buchwald, V. F. (1975). Handbook of Iron Meteorites. University of California Press, 1418 pp. evols.library.manoa.hawaii.edu/handle/10524/35673.

Budde, G., Burkhardt, C., Brennecka, G. A., Fischer-Gödde, M., Kruijer, T. S., & Kleine, T. (2016). Molybdenum isotopic evidence for the origin of chondrules and a distinct genetic heritage of carbonaceous and non-carbonaceous meteorites. *Earth and Planetary Science Letters*, *454*, 293-303.

Chabot, N. L., & Jones, J. H. (2003). The parameterization of solid metal-liquid metal partitioning of siderophile elements. Meteoritics & Planetary Science, 38(10), 1425-1436.

Fouché, K. F., & Smales, A. A. (1966). The distribution of gold and rhenium in iron meteorites. *Chemical Geology*, *1*, 329-339.

Goldstein, J. I., & Doan Jr, A. S. (1972). The effect of phosphorus on the formation of the Widmanstätten pattern in iron meteorites. *Geochimica et Cosmochimica Acta*, *36*(1), 51-69.

Kruijer, T. S., Burkhardt, C., Budde, G., & Kleine, T. (2017). Age of Jupiter inferred from the distinct genetics and formation times of meteorites. *Proceedings of the National Academy of Sciences*, 201704461.

Ludwig, K. R. (2003). Users manual for ISOPLOT/EX, version 3. A geochronological toolkit for Microsoft Excel. *Berkeley Geochronology Center Special Publication*, (4).

McCoy, T. J., Walker, R. J., Goldstein, J. I., Yang, J., McDonough, W. F., Rumble, D., ... & Kotula, P. G. (2011). Group IVA irons: New constraints on the crystallization and cooling history of an asteroidal core with a complex history. *Geochimica et Cosmochimica Acta*, 75(22), 6821-6843.

Poole, G. M., Rehkämper, M., Coles, B. J., Goldberg, T., & Smith, C. L. (2017). Nucleosynthetic molybdenum isotope anomalies in iron meteorites–new evidence for thermal processing of solar nebula material. *Earth and Planetary Science Letters*, *473*, 215-226.

Rusk, B. (2009). Laser Ablation ICP-MS in the Earth Sciences: Current Practices and Outstanding Issues. *Economic Geology*, 104(4), 601-602.

Scott, E. R., & Wasson, J. T. (1975). Classification and properties of iron meteorites. *Reviews of Geophysics*, *13*(4), 527-546.

Scott, E. R., & Wasson, J. T. (1976). Chemical classification of iron meteorites—VIII. Groups IC. IIE, IIIF and 97 other irons. *Geochimica et Cosmochimica Acta*, *40*(1), 103-115.

Wasson, J. T. (1969). The chemical classification of iron meteorites—III. Hexahedrites and other irons with germanium concentrations between 80 and 200 ppm. *Geochimica et Cosmochimica Acta*, *33*(7), 859-876.

Wasson, J. T. (1999). Trapped melt in IIIAB irons; solid/liquid elemental partitioning during the fractionation of the IIIAB magma. *Geochimica et Cosmochimica Acta*, *63*(18), 2875-2889.

Walker, R. J., McDonough, W. F., Honesto, J., Chabot, N. L., McCoy, T. J., Ash, R. D., & Bellucci, J. J. (2008). Modeling fractional crystallization of group IVB iron meteorites. *Geochimica et Cosmochimica Acta*, *72*(8), 2198-2216.

Appendix I

Isotopes used for LA-ICP-MS:

^{31}P, ^{51}V, ^{53}Cr, ^{55}Mn, ^{57}Fe, ^{59}Co, ^{61}Ni, ^{63}Cu, ^{66}Zn, ^{71}Ga, ^{73}Ge, ^{75}As, ^{95}Mo, ^{99}Ru, ^{101}Rh, ^{108}Pd, ^{121}Sb, ^{183}W,^{185}Re, ^{189}Os, ^{193}Ir, ^{195}Pt, ^{197}Au